

Dynamic range and linearity improvement for zero-field single-beam atomic magnetometer

Kai-Feng Yin(尹凯峰), Ji-Xi Lu(陆吉玺), Fei Lu(逯斐), Bo Li(李博),Bin-Quan Zhou(周斌权), and Mao Ye(叶茂)

Citation: Chin. Phys. B, 2022, 31 (**11**): 110703. DOI: 10.1088/1674-1056/ac6010

What follows is a list of articles you may be interested in

Magnetic shielding property for cylinder with circular, square, and equilateral triangle holes

Si-Yuan Hao(郝思源), Xiao-Ping Lou(娄小平), Jing Zhu(祝静), Guang-Wei Chen(陈广伟), and Hui-Yu Li(李慧宇)
Chin. Phys. B, 2021, 30 (**6**): 060702. DOI: 10.1088/1674-1056/abeeee

A modified analytical model of the alkali-metal atomic magnetometer employing longitudinal carrier field

Chang Chen(陈畅), Yi Zhang(张燚), Zhi-Guo Wang(汪之国), Qi-Yuan Jiang(江奇渊), Hui Luo(罗晖), and Kai-Yong Yang(杨开勇)
Chin. Phys. B, 2021, 30 (**5**): 050707. DOI: 10.1088/1674-1056/abd7d3

Search for topological defect of axionlike model with cesium atomic comagnetometer

Yucheng Yang(杨雨成), Teng Wu(吴腾), Jianwei Zhang(张建玮), and Hong Guo(郭弘)
Chin. Phys. B, 2021, 30 (**5**): 050704. DOI: 10.1088/1674-1056/abf132

Atomic magnetometer with microfabricated vapor cells based on coherent population trapping

Xiaojie Li(李晓杰), Yue Shi(史越), Hongbo Xue(薛洪波), Yong Ruan(阮勇), and Yanying Feng(冯焱颖)
Chin. Phys. B, 2021, 30 (**3**): 030701. DOI: 10.1088/1674-1056/abc2b9

Miniature quad-channel spin-exchange relaxation-free magnetometer for magnetoencephalography

Jian-Jun Li(李建军), Peng-Cheng Du(杜鹏程), Ji-Qing Fu(伏吉庆), Xu-Tong Wang(王旭桐), Qing Zhou(周庆), Ru-Quan Wang(王如泉)
Chin. Phys. B, 2019, 28 (**4**): 040703. DOI: 10.1088/1674-1056/28/4/040703

Dynamic range and linearity improvement for zero-field single-beam atomic magnetometer

Kai-Feng Yin(尹凯峰)[1], Ji-Xi Lu(陆吉玺)[2,3,†], Fei Lu(逯斐)[1,2], Bo Li(李博)[3], Bin-Quan Zhou(周斌权)[2], and Mao Ye(叶茂)[2,3,‡]

[1] *School of Instrumentation Science and Optoelectronics Engineering, Beihang University, Beijing* 100191, *China*
[2] *Research Institute for Frontier Science, Beihang University, Beijing* 100191, *China*
[3] *Beihang Hangzhou Innovation Institute Yuhang, Xixi Octagon City, Hangzhou* 310023, *China*

(Received 26 December 2021; revised manuscript received 22 March 2022; accepted manuscript online 23 March 2022)

Zero-field single-beam atomic magnetometers with transverse parametric modulation for ultra-weak magnetic field detection have attracted widespread attention recently. In this study, we present a comprehensive response model and propose a modification method of conventional first harmonic response by introducing the second harmonic correction. The proposed modification method gives improvement in dynamic range and reduction of linearity error. Additionally, our modification method shows suppression of response instability caused by optical intensity and frequency fluctuations. An atomic magnetometer with single-beam configuration is built to compare the performance between our proposed method and the conventional method. The results indicate that our method's magnetic field response signal achieves a 5-fold expansion of dynamic range from 2 nT to 10 nT, with the linearity error decreased from 5% to 1%. Under the fluctuations of 5% for optical intensity and ±15 GHz detuning of frequency, the proposed modification method maintains intensity-related instability less than 1% and frequency-related instability less than 8% while the conventional method suffers 15% and 38%, respectively. Our method is promising for future high-sensitive and long-term stable optically pumped atomic sensors.

Keywords: atomic magnetometer, dynamic range, linearity error, response signal stability

PACS: 07.07.Df, 07.55.Ge, 06.20.fb, 32.30.Dx **DOI:** 10.1088/1674-1056/ac6010

1. Introduction

Optically-pumped magnetometers (OPMs) based on the detection of spin polarization of optically polarized atoms have raised widespread interest in recent years. Zero-field atomic magnetometers operated in the regime of spin-exchange-relaxation-free (SERF) have reported extraordinary sensitivity of sub-femtotesla,[1,2] and are widely applied in testing of materials, fundamental physics including the measurement of the permanent electric dipole moment, and bio-magnetic measurements.[3–6] To date, atomic magnetometers featured in miniaturization, high sensitivity and cryogen-free have become promising alternatives to superconductor quantum interference device (SQUID) magnetometers in bio-magnetic measurements such as magnetoencephalography (MEG) and magnetocardiography (MCG).[7,8]

Atomic magnetometers operated in zero-field are implemented in many configurations to satisfy the various applications, including magnetometers based on crossed pump-probe beams,[9–11] nearly parallel pump-probe beams,[12] single elliptically polarized light,[13,14] single circularly polarized light,[15,16] as well as schemes with multi-channel[17,18] and gradiometer.[19] Among these configurations, single-beam magnetometers have been widely applied in MEG and MCG with considerably less cost and reduction of volume.[20–22] The ambient magnetic field would induce the precession of the spin polarization, resulting in light absorption or polarization changes in alkali vapor, which forms the basis of the single-beam atomic magnetometer. In the single-beam configuration, it is a conventional practice that the magnetic field can be measured using the demodulated first harmonic signal by applying the transverse parametric modulation on the spin polarization.[23,24] The demodulated first harmonic dispersive signal limits the magnetometer's dynamic range typically at 2 nT with 5% linearity error,[25] restricting the application scenarios of atomic magnetometers. Meanwhile, the instability of the response signal caused by linearity error decreases the accuracy in source imaging, which is critical for OPM-MEG.[26] Although atomic magnetometers with active closed-up operation show the dynamic range of 10 nT with 5% linearity error, the compensating magnetic field generated by the closed-up operation will introduce the cross-talk between adjacent magnetometers.[27]

This study begins with investigating the response signal to the magnetic field in zero-field single-beam magnetometers and proposes a response modification method of the first harmonic response by introducing the second harmonic correction. Our method shows the capability to expand the dynamic range and reduce the linearity error. Furthermore, by sup-

†Corresponding author. E-mail: lujixi@buaa.edu.cn
‡Corresponding author. E-mail: maoye@buaa.edu.cn

© 2022 Chinese Physical Society and IOP Publishing Ltd

pressing the influence of optical intensity and frequency, the response signal remains stable under optical intensity and frequency fluctuations. Finally, the experiments are carried out to evaluate the proposed modification method's performance in dynamic range, linearity and response signal stability.

2. Methods

Zero-field atomic magnetometer works with the polarized atoms created by optical pumping. The spin polarization evolved under the combined effects of optical pumping, spin relaxation, and magnetic field induced precession. In the SERF regime when the spin-exchange rate is much larger than the Larmor precession frequency, the evolution of spin polarization can be described with the Bloch equation

$$\frac{\mathrm{d}\boldsymbol{P}}{\mathrm{d}t} = \frac{1}{q}\left[\gamma \boldsymbol{B}\times\boldsymbol{P} + R_{\mathrm{op}}\left(s\cdot\boldsymbol{z}-\boldsymbol{P}\right) - R_{\mathrm{rel}}\boldsymbol{P}\right], \tag{1}$$

where $\boldsymbol{P}$ is the spin polarization vector, q is the slowing-down factor, γ is the electron gyromagnetic ratio, s is the photon polarization of the pump beam, R_{op} is the optical pumping rate, and R_{rel} is the relaxation rate mainly caused by spin-destruction and wall-collisions. The circularly polarized light at D1 line propagates along the z-axis and the transmission obeys[28,29]

$$\frac{I}{I_0} = \exp\left[-\kappa\left(P_z,\nu\right)\right], \tag{2}$$

where I is the transmitted light intensity, I_0 is the incident intensity, P_z is the z-axis projection of $\boldsymbol{P}$, and ν is the incident optical frequency. Equation (2) shows the basis of polarization measurement through light intensity detection. Optical depth $\kappa(P_z,\nu)$ that depends on spin polarization P_z and incident optical frequency ν can be expressed as[30]

$$\begin{aligned}\kappa(P_z,\nu) &= nL\left(1-P_z\right)\kappa_0\mathcal{L}\left(\Delta\nu\right),\\ \mathcal{L}\left(\Delta\nu\right) &= \frac{\Gamma_{\mathrm{D1}}/2}{(\Delta\nu)^2+(\Gamma_{\mathrm{D1}}/2)^2},\end{aligned} \tag{3}$$

where n is the number density of the alkali atoms, L is the light propagation length in the vapor cell, κ_0 is the absorption coefficient of alkali atoms at resonance, $\mathcal{L}\left(\Delta\nu\right)$ is the Lorentzian function related to frequency detuning $\Delta\nu = \nu - \nu_{\mathrm{D1}}$, and Γ_{D1} is the pressure broadened optical width. The relationship between transmitted light intensity I and the spin polarization P_z can be described by first-order approximation at P_0 $(0<P_0<1)$

$$\begin{aligned}I(P_z) &= \exp[-nL\kappa_0\mathcal{L}(\Delta\nu)(1-P_0)]I_0\\ &\quad+\exp[-nL\kappa_0\mathcal{L}(\Delta\nu)(1-P_0)]\\ &\quad\times nL\kappa_0\mathcal{L}(\Delta\nu)I_0(P_z-P_0).\end{aligned} \tag{4}$$

As shown in Eq. (4), the attenuation of the incident light in the vapor cell can provide information about the spin projection along the z-axis. In our single-beam configuration, a transverse modulation magnetic field $B_{\mathrm{mod}}\sin(\omega_{\mathrm{mod}}t)$ was applied along the y-axis. Therefore the components of total magnetic field $\boldsymbol{B}$ were $B_x = B_{x0}$, $B_y = B_{\mathrm{mod}}\sin(\omega_{\mathrm{mod}}t)+B_{y0}$, and $B_z = B_{z0}$, where B_{x0}, B_{y0}, and B_{z0} are the residual environment magnetic field components. By solving Eq. (1), the spin polarization along the z-axis is[23,24]

$$P_{z-\omega} = \frac{2R_{\mathrm{op}}\gamma\sin(\omega_{\mathrm{mod}}t)}{\gamma^2B_{y0}^2+\left(R_{\mathrm{op}}+R_{\mathrm{rel}}\right)^2}J_0\left(u\right)J_1\left(u\right)\cdot B_{y0}, \tag{5}$$

$$P_{z-2\omega} = \frac{2R_{\mathrm{op}}\left(R_{\mathrm{op}}+R_{\mathrm{rel}}\right)\cos(2\omega_{\mathrm{mod}}t)}{\gamma^2B_{y0}^2+\left(R_{\mathrm{op}}+R_{\mathrm{rel}}\right)^2}J_0\left(u\right)J_2\left(u\right), \tag{6}$$

where J_n $(n=0,1,2)$ is the n-order Bessel function of the first kind, and $u = \gamma B_{\mathrm{mod}}/q\omega_{\mathrm{mod}}$ is the modulation index. Consequently, by combining Eqs. (4)–(6), we can get the demodulation voltage signals at the first and second harmonic

$$\begin{aligned}V_\omega(B_{y0}) &= G_1K_1S_{\mathrm{PD}}K_2(I_0,\nu)\\ &\quad\times\frac{R_{\mathrm{op}}\gamma}{\gamma^2B_{y0}^2+\left(R_{\mathrm{op}}+R_{\mathrm{rel}}\right)^2}J_0\left(u\right)J_1\left(u\right)\cdot B_{y0},\end{aligned} \tag{7}$$

$$\begin{aligned}V_{2\omega}(B_{y0}) &= G_2K_1S_{\mathrm{PD}}K_2(I_0,\nu)\\ &\quad\times\frac{R_{\mathrm{op}}\left(R_{\mathrm{op}}+R_{\mathrm{rel}}\right)}{\gamma^2B_{y0}^2+\left(R_{\mathrm{op}}+R_{\mathrm{rel}}\right)^2}J_0\left(u\right)J_2\left(u\right),\end{aligned} \tag{8}$$

where G_1 and G_2 are the output voltage gain factors for different channels of the lock-in amplifier, K_1 is the current–voltage conversion coefficient of transimpedance amplifier, S_{PD} is the photosensitivity of photodiodes, and K_2 is a conversion coefficient between transmitted light intensity and spin polarization P_z

$$K_2\left(I_0,\nu\right) = \exp\left[-nL\kappa_0\mathcal{L}(\Delta\nu)(1-P_0)\right]nLI_0\kappa_0\mathcal{L}\left(\Delta\nu\right). \tag{9}$$

The conventional first harmonic response signal is affected by the incident optical intensity I_0, frequency ν and the modulation index u as indicated in Eq. (7). Based on Eqs. (7) and (8), we introduce the modification method with the correction of the second harmonic response and the corresponding response signal is

$$V_{\mathrm{MOD}}\left(B_{y0}\right) = \frac{V_\omega}{V_{2\omega}} = \frac{G_1}{G_2}\frac{\gamma}{R_{\mathrm{op}}+R_{\mathrm{rel}}}\cdot\frac{J_1\left(u\right)}{J_2\left(u\right)}\cdot B_{y0}. \tag{10}$$

As indicated in Eq. (10), response signal V_{MOD} shows the improved dynamic range and lower linearity error to B_{y0} for eliminating the nonlinear term $\gamma^2B_{y0}^2$ in V_ω. Meanwhile, in contrast to the first harmonic signal V_ω, terms K_1, S_{PD}, $K_2(I_0,\nu)$ are removed in V_{MOD}, which gives a more stable response signal by suppressing the influence of optical intensity I_0 and frequency ν fluctuations. In summary, the proposed modification method promises an accurate and stable response signal in a larger measurement range of magnetic fields.

3. Experimental setup and procedures

A potassium spherical glass vapor cell with a diameter of 10 mm was filled with 1.8 amg ^{4}He and 0.1 amg N_2. The N_2 acted as the quenching gas to prevent the radiation trapping while the ^{4}He efficiently decreased the effect of wall collisions. The vapor cell was electrically heated to 170 °C by a printed double-layer resistance wire, generating an atomic number density of 4.97×10^{13} cm^{-3} according to Ref. [31]. The heating resistance wire was specially designed to make the current flow in opposite directions between adjacent wires to eliminate the heating-current-induced magnetic field. The vapor cell temperature was stabilized by a proportional-integral-derivative (PID) controller at an accuracy of ±0.02 °C, and the accuracy was obtained by a non-magnetic Pt-1000 temperature sensor that closed to the vapor cell.

The experiments were carried out on a single-beam atomic magnetometer, as shown in Fig. 1. The optical pumping beam was generated from an external-cavity diode laser (ECDL, New Focus TLB-6813), and carried into the magnetometer through a single-mode polarization-maintaining fiber. The optical frequency was tuned and locked to the D1 line of potassium at 770.1033 nm (389.2886 THz) by the feedback of a wavelength meter (HighFinesse WS-7). An acousto-optic modulator (AOM, G&H 3080-125) was placed in front of the optical fiber to modulate the light and generate artificial intensity fluctuations. The light emitted from the fiber was expanded and collimated to a diameter of 4 mm, then passed through the polarizer and quarter-wave plate in sequence. The incident intensity $I_0 = 6.35$ mW/cm^2 traversed through the vapor cell along z-direction and was finally exposed to the photodiode. The photosensitivity S_{PD} of the photodiode was about 0.55 A/W at 389.2886 THz.

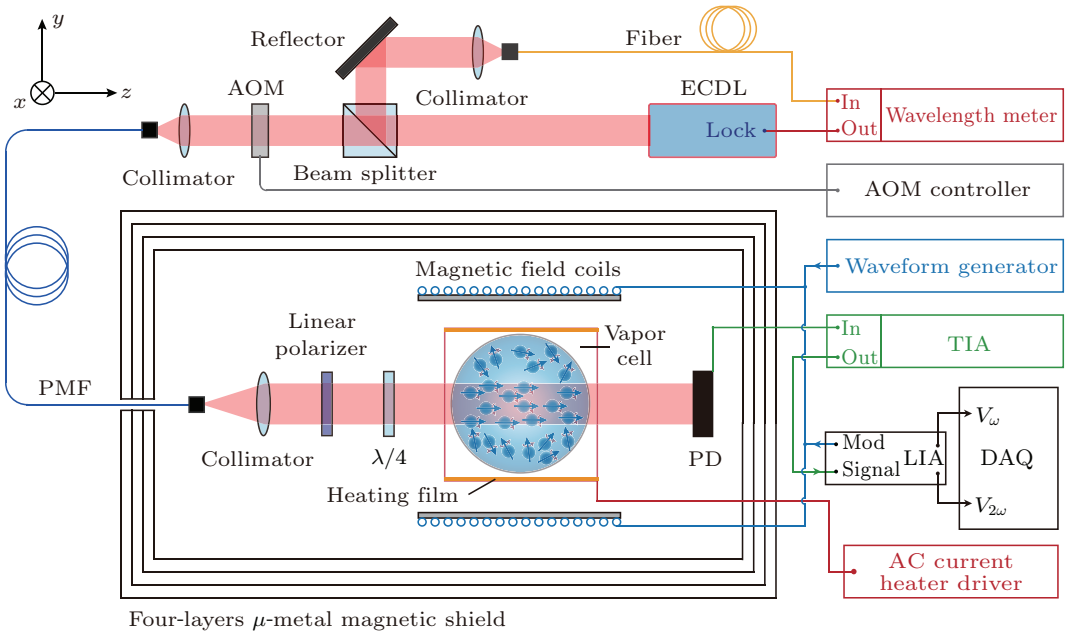


Fig. 1. Schematic of the experimental apparatus. ECDL: external-cavity diode laser, TIA: transimpedance amplifier, LIA: lock-in amplifier, PD: silicon photodiode, DAQ: data acquisition system, $\lambda/4$: quarter-wave plate, AOM: acousto-optic modulator, PMF: polarization-maintaining fiber.

The atomic magnetometer was placed inside a four-layers μ-metal magnetic shield, and the internal residual magnetic field was below 2 nT. Before running the experiment, the magnetic field surrounding the vapor cell was compensated to near zero-field (typically below 1 pT) by triaxial magnetic field coils integrated inside the magnetometer driven by the waveform generators (Keysight 33522B). The response signal V_ω, $V_{2\omega}$ to magnetic field B_{y0} was extracted using the digital lock-in amplifier (Zurich Instruments MFLI) following the process: the lock-in amplifier generated the modulation voltage signal $V_{\rm mod}\sin(\omega_{\rm mod}t)$ and applied to the y-axis coil through a series resistance to produce the modulation magnetic field $B_{\rm mod}\sin(\omega_{\rm mod}t)$ where $B_{\rm mod} = 110$ nT, $\omega_{\rm mod} = 900$ Hz; the spin polarization evolved in the modulation magnetic field, yielding the variation of transmitted light intensity I as indicated in Eq. (4); the corresponding light intensity variations were detected by a silicon photodiode and converted to the voltage signal by the transimpedance amplifier (Thorlabs PDA200C) with conversion coefficient K_1 subsequently; this voltage signal was finally sent to the lock-in amplifier for demodulation at first and second harmonic, generating the corresponding voltage response V_ω and $V_{2\omega}$ with gain factor G_1 and G_2, respectively. In practice, we made $G_1 = G_2$ in the subsequent experiments.

To investigate the magnetometer's dynamic range and linearity, a sweep magnetic field ranging in ± 30 nT was applied to the y-axis coil. The corresponding response voltages V_ω and $V_{2\omega}$ were recorded simultaneously with B_{y0} by the data acquisition system (NI PXIe-4464) at the sampling rate of 1 kHz. Furthermore, to estimate the stability of mag-

netometer's response signal under optical intensity and frequency fluctuations, the artificial variations were applied to the incident light. For optical intensity fluctuations, a 40 mVpp triangular modulation at 1 Hz was applied to the AOM, generating a 5% variation of optical intensity, resulting in I_0 varying from 6.2 mW/cm^2 to 6.51 mW/cm^2 periodically. For optical frequency fluctuations, by controlling the piezoelectric transducer (PZT) voltage inside the ECDL, the incident optical frequency was varied at ν 389.2886 THz$\pm$15 GHz. Additionally, a 100 pT sinusoidal calibration magnetic field at 31 Hz was applied along the y-axis, and the corresponding peak-to-peak amplitude in the response signal was extracted to evaluate the signal stability under optical intensity and frequency fluctuations.

4. Results and discussion

4.1. Dynamic range and linearity

As shown in Fig. 2, the first and second harmonic signals V_ω and $V_{2\omega}$ extracted from the lock-in amplifier were illustrated with black and blue lines. The modification response in Fig. 2 with the red line referred to the response signal calculated through our modification method as indicated in Eq. (10). By adjusting the voltage gain factor G_1 and G_2, the modification response was made consistently with the first harmonic response to the same magnetic field B_{y0}.

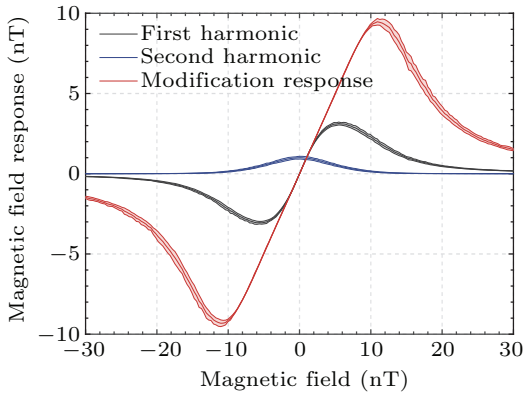


Fig. 2. The first harmonic (black line) and second harmonic (blue line) responses of the magnetic field B_{y0} and the modification response (red line) calculated from Eq. (10). The shaded areas of the curves indicated multiple measurement errors.

Contrary to expectations, the modification response appeared a dispersive feature to B_{y0} similarly to the first harmonic signal, rather than linearly to B_{y0} as expected. Thus, the relaxation mechanism related to B_{y0} should be further investigated in our modification method. Previous studies[32,33] show that the spin-exchange relaxation rate $R_2^{\rm SE}$ is in quadratic relationship with the magnetic field ($R_2^{\rm SE} \sim (\gamma B_{y0})^2 \cdot T_{\rm SE}$), thus $R_2^{\rm SE}$ can be shown as

$$R_2^{\rm SE}(B_{y0}) = k_{\rm SE} \cdot (\gamma B_{y0})^2 \cdot T_{\rm SE}, \tag{11}$$

where $k_{\rm SE}$ is the scale factor, and $T_{\rm SE}$ is the transverse relaxation time of the spin ensemble. Accordingly, by considering the relaxation rate $R_2^{\rm SE}$ caused by B_{y0}, the response signal of our modification method was expressed as follows:

$$V_{\rm MOD}(B_{y0}) = \frac{\gamma}{R_{\rm op} + R_{\rm rel} + k_{\rm SE} \cdot (\gamma B_{y0})^2 \cdot T_{\rm SE}} \cdot \frac{J_1(u)}{J_2(u)} \cdot B_{y0}. \tag{12}$$

To quantify the deviation between the response signal $S_{\rm response}$ and the ideal output signal $S_{\rm signal}$, we introduced the concept of linearity error $\delta_{\rm L}$ defined as[34]

$$\delta_{\rm L} = \frac{S_{\rm response} - S_{\rm signal}}{S_{\rm signal}} \times 100\%. \tag{13}$$

Referring to the study by Rea *et al.*,[26] the dynamic range of the atomic magnetometer was defined as the measurement range where the linearity error was less than 5%. As shown in Fig. 3(a) with the shaded region, the calibrated first harmonic response showed the dynamic range of 2 nT, while the modification response remained a linear response over the range of 10 nT.

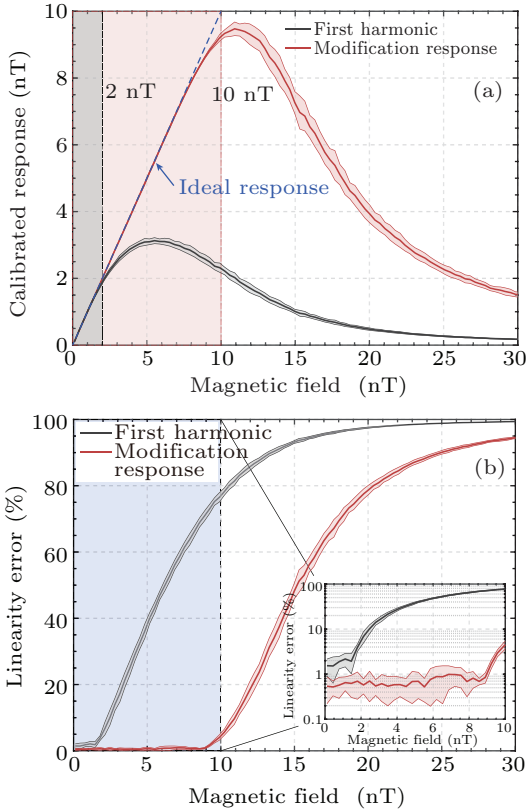


Fig. 3. (a) Calibrated response of conventional first harmonic (black line) and modification response (red line); (b) linearity error of both conventional model (black line) and modification model (red line); inset: linearity error within 10 nT range with y-axis in logarithmic scale.

Figure 3(b) demonstrated the linearity error $\delta_{\rm L}$ comparison of the first harmonic V_ω and modification response $V_{\rm MOD}$. It was apparent that the linearity error of the first harmonic response increased rapidly when the magnetic field exceeded

its dynamic range of 2 nT, while the modification response maintained its linearity within 10 nT. Notably, the modification response showed a relatively small linearity error within the dynamic range of 10 nT, giving $\delta_L < 1\%$ as shown in the inset.

4.2. Response signal stability

The proposed modification response V_{MOD} showed the suppression of response instability induced by optical intensity I_0 and frequency ν fluctuations as indicated in Eq. (12). Firstly, the response signal stability was investigated by applying artificial fluctuations on optical intensity.As indicated in Fig. 4, the first harmonic and modification responses were recorded with black and red lines, against the variation of 5% in optical intensity with the blue line. It was seen from the figure that the instability of the first harmonic influenced by optical intensity fluctuations was suppressed in our modification method, which gave a stable response signal as shown with the red line.

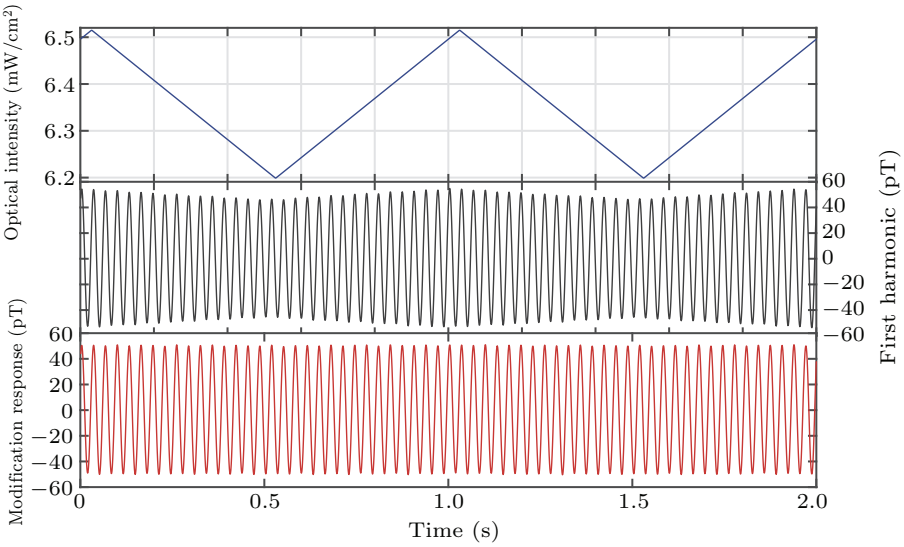


Fig. 4. First harmonic (black line) and the modification response curves (red line) to 100 pT sinusoidal magnetic field at 31 Hz under the 5% optical intensity fluctuations (blue line).

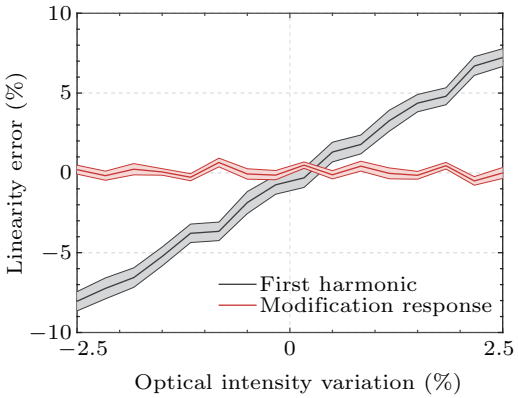


Fig. 5. Linearity error of the first harmonic response (red line) and modification response (black line) induced by optical intensity fluctuations calculated by Eq. (13).

Moreover, the linearity error was taken to quantify the suppression of optical intensity fluctuations. The peak-to-peak amplitude of the response signal in a period was taken as $S_{response}$ for both first harmonic V_ω and modification response V_{MOD} and S_{signal} was the averaged peak-to-peak amplitude of V_ω and V_{MOD} during the measurement time, respectively. As shown in Fig. 5, the first harmonic response suffered a 15% variation and showed a trend consistent with optical intensity fluctuations. As a comparison, the linearity error of modification response was maintained lower than 1%, independent from the influence of optical intensity fluctuations.

Meanwhile, to estimate the consistency of the response signal under optical intensity fluctuations, we calculated the peak-to-peak amplitude standard deviations of V_ω and V_{MOD} in 100 seconds, respectively. The standard deviation of the first harmonic V_ω reached 4.75 pT when the 100 pT at 31 Hz sinusoidal calibration magnetic field was applied. In comparison, the standard deviation of V_{MOD} was 0.42 pT, which gave a reliable and accurate response signal when optical intensity fluctuations existed.

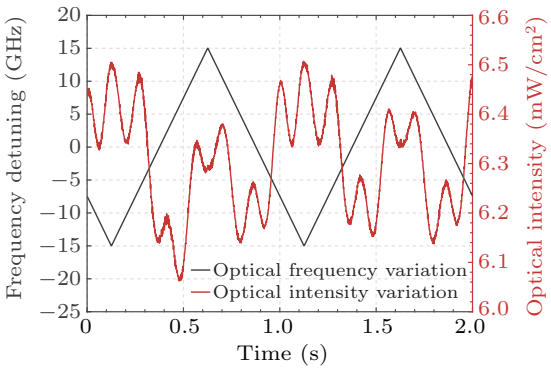


Fig. 6. Modulation on the incident optical frequency with 1 Hz triangular wave (black line) and the accompanied optical intensity noise (red line).

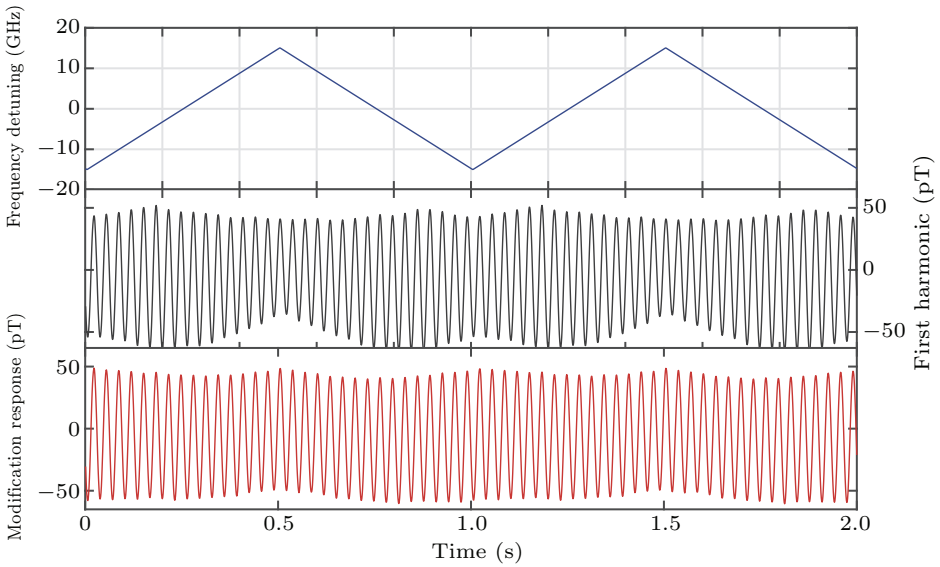


Fig. 7. First harmonic response (black line) and the modification response (red line) to the 100 pT sinusoidal magnetic field at 31 Hz under the influence of the optical frequency fluctuations at ±15 GHz (blue line).

Moreover, the influence of optical frequency fluctuations on the response signal was studied. By controlling the PZT voltage inside the ECDL, a linear optical frequency variation of 389.2886 THz ± 15 GHz was obtained, accompanied by undesired optical intensity noise, as shown in Fig. 6. The unexpected optical intensity fluctuations were caused by the limitation of the ECDL, but they would not have fatal impacts on subsequent analysis.

As shown in Fig. 7, with the combined influence of optical frequency and intensity fluctuations, the first harmonic response V_ω changed significantly while the modification response V_{MOD} showed slight variations. The linearity error δ_{L} of the first harmonic response varied 38% under the optical frequency fluctuations, as demonstrated in Fig. 8. On the contrary, the modification response maintained a level of 8% under the combined effects of optical intensity and frequency variations. In addition, the asymmetry of the linearity error between ±15 GHz frequency detuning in Fig. 8 was because the magnetometer worked with the slight frequency detuning (about 7 GHz redshift in our experiment) for the optimal performance.

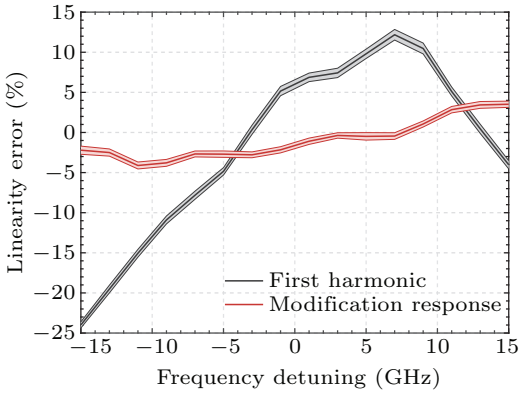


Fig. 8. First harmonic (red line) and modification (black line) linearity error caused by optical frequency variation.

Finally, the noise spectral density averaged for 2 minutes of both the first harmonic V_ω (in red line) and the modification response V_{MOD} (in red dashed line) was shown in Fig. 9. As seen, the noise spectral density of the proposed modification response was 8 fT/Hz$^{1/2}$, which may be limited by the magnetic noise of the magnetic shield,[35] consistently with the first harmonic response signal.

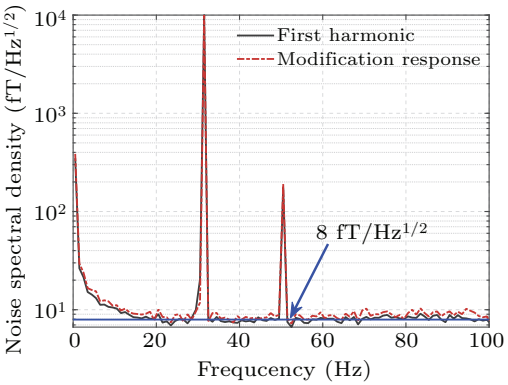


Fig. 9. Noise spectral densities of the conventional response and our modification method. The peak at 31 Hz was the calibration signal we applied, the peak at 50 Hz Hz was the power frequency of the environment, and the blue line was a fit to the atomic magnetometer noise floor.

5. Conclusion

In this study, we develop a comprehensive response model for magnetic field measurement in zero-field single-beam atomic magnetometer. Then the modification method for magnetometer's response that introduces the second harmonic correction is proposed, which is advantageous in dynamic range expansion, linearity error reduction, and response signal stability. The experiments showed that the dynamic range was expanded to 10 nT, 5-fold larger than 2 nT in the conventional method. Furthermore, the linearity error of the proposed method was maintained at 1% in the dynamic range,

five times lower than the first harmonic response. In addition, when optical intensity fluctuated at 5% and frequency detuned between ± 15 GHz, the response signal was maintained at intensity-related bias less than 1% and frequency-related bias less than 8%, whereas the conventional method suffers instability of 15% and 38%, respectively.

Additionally, the modified response is as sensitive as the first harmonic signal, ensuring high-sensitive and accurate magnetic field measurement. Furthermore, our modification method operated in real-time without introducing extra interferences to the environment, which is advantageous for the applications of MEG and MCG, where sensor arrays are utilized.

Acknowledgements

The authors would like to give special thanks to Feifan Tan for her encouragement.

Project supported by the National Key R&D Program of China (Grant No. 2018YFB2002405) and the National Natural Science Foundation of China (Grant No. 61903013).

References

[1] Kominis I K, Kornack T W, Allred J C and Romalis M V 2003 *Nature* **422** 596
[2] Dang H B, Maloof A C and Romalis M V 2010 *Appl. Phys. Lett.* **97** 151110
[3] Brookes M J, Boto E, Rea M, Shah V, Osborne J, Holmes N, Hill R M, Leggett J, Rhodes N and Bowtell R 2021 *NeuroImage* **236** 118025
[4] Abel C, Afach S, Ayres N J, *et al.* 2020 *Phys. Rev. Lett.* **124** 081803
[5] Romalis M V and Dang H B 2011 *Mater. Today* **14** 258
[6] Du P C, Li J J, Yang S J, Wang X T, Zhuo Y, Wang F and Wang R Q 2019 *Chin. Phys. B* **28** 040702
[7] Knappe S, Sander T H, Kosch O, Wiekhorst F, Kitching J and Trahms L 2010 *Appl. Phys. Lett.* **97** 133703
[8] Boto E, Holmes N, Leggett J, Roberts G, Shah V, Meyer S S, Mu noz L D, Mullinger K J, Tierney T M, Bestmann S, Barnes G R, Bowtell R and Brookes M J 2018 *Nature* **555** 657
[9] Fu J Q, Du P C, Zhou Q and Wang R Q 2016 *Chin. Phys. B* **25** 010302
[10] Qiu X Y, Xu Z Y, Peng X X, Li L H, Zhou Y M, Wei M M, Zhou M and Xu X Y 2020 *Appl. Phys. Lett.* **116** 034001
[11] Zhang J H, Liu Q, Zeng X J, Li J X and S W M 2012 *Chin. Phys. Lett.* **29** 068501
[12] Karaulanov T, Savukov I and Kim Y J 2016 *Meas. Sci. Technol.* **27** 055002
[13] Shah V and Romalis M V 2009 *Phys. Rev. A* **80** 013416
[14] Zheng W Q, Su S R, Zhang G Y, Bi X and Lin Q 2020 *Biomed. Opt. Express* **11** 649
[15] Savukov I, Kim Y J, Shah V and Boshier M G 2017 *Meas. Sci. Technol.* **28** 035104
[16] Liu G, Tang J J, Yin Y, Wang Y X, Zhou B Q and Han B C 2020 *IEEE Sens. J.* **20** 5827
[17] Fang X J, Wei K, Zhao T, Zhai Y Y, Ma D Y, Xing B Z, Liu Y and Xiao Z S 2020 *Opt. Express* **28** 26447
[18] Colombo A P, Carter T R, Borna A, Jau Y Y, Johnson C N, Dagel A L and Schwindt P D D 2016 *Opt. Express* **24** 15403
[19] Sulai I A, DeLand Z J, Bulatowicz M D, Wahl C P, Wakai R T and Walker T G 2019 *Rev. Sci. Instrum.* **90** 085003
[20] Sheng D, Perry A R, Krzyzewski S P, Geller S, Kitching J and Knappe S 2017 *Appl. Phys. Lett.* **110** 031106
[21] Sander T H, Preusser J, Mhaskar R, Kitching J, Trahms L and Knappe S 2012 *Biomed. Opt. Express* **3** 981
[22] Iivanainen J, Zetter R, Grön M, Hakkarainen K and Parkkonen L 2019 *NeuroImage* **194** 244
[23] Wang J, Fan W F, Yin K F, Yan Y G, Zhou B Q and Song X D 2020 *Phys. Rev. A* **101** 053427
[24] Li Z M, Wakai R T and Walker T G 2006 *Appl. Phys. Lett.* **89** 134105
[25] Boto E, Meyer S S, Shah V, Alem O, Knappe S, Kruger P, Fromhold T M, Lim M, Glover P M, Morris P G, Bowtell R, Barnes G R and Brookes M J 2017 *NeuroImage* **149** 404
[26] Rea M, Holmes N, Hill R M, Boto E, Leggett J, Edwards L J, Woolger D, Dawson E, Shah V, Osborne J, Bowtell R and Brookes M J 2021 *NeuroImage* **241** 118401
[27] Nardelli N V, Perry A R, Krzyzewski S P and Knappe S 2020 *EPJ Quantum Technol.* **7** 11
[28] Breschi E and Weis A 2012 *Phys. Rev. A* **86** 053427
[29] Castagna N and Weis A 2011 *Phys. Rev. A* **84** 053421
[30] Seltzer, S J 2008 *Developments in Alkali-Metal Atomic Magnetometry*, Ph. D. Dissertation (New Jersey: Princeton University)
[31] Alcock C B, Itkin V P and Horrigan M K 1984 *Can. Metall. Q.* **23** 309
[32] Shah V and Romalis M V 2009 *Phys. Rev. A* **80** 013416
[33] Savukov I M and Romalis M V 2005 *Phys. Rev. A* **71** 023405
[34] Regtien P and Dertien E 2018 *Sensors for Mechatronics*, 2nd edn. (Amsterdam: Elsevier) pp.40-41
[35] Ma D Y, Lu J X, Fang X J, Yang K, Wang K, Zhang N, Han B C and Ding M 2022 *IEEE Trans. Ind. Electron.* **69** 991